Carbohydrate Polymers 112 (2014) 432–439

Contents lists available at ScienceDirect

Carbohydrate Polymers

journal homepage: www.elsevier.com/locate/carbpol

Rheological properties of micro-/nanofibrillated cellulose suspensions: Wall-slip and shear banding phenomena

Oleksandr Nechyporchuk[a,b,c,d,e], Mohamed Naceur Belgacem[c,d,e], Frédéric Pignon[a,b,*]

[a] Univ. Grenoble Alpes, LRP, F-38000 Grenoble, France
[b] CNRS, LRP, F-38000 Grenoble, France
[c] Univ. Grenoble Alpes, LGP2, F-38000 Grenoble, France
[d] CNRS, LGP2, F-38000 Grenoble, France
[e] Agefpi

ARTICLE INFO

Article history:
Received 19 March 2014
Received in revised form 2 May 2014
Accepted 31 May 2014
Available online 8 June 2014

Keywords:
Rheology
Nanofibrillated cellulose (NFC)
Microfibrillated cellulose (MFC)
Cellulose nanofibers (CNF)
Wall-slip
Shear banding

ABSTRACT

The rheological properties of enzymatically hydrolyzed and TEMPO-oxidized microfibrillated/nanofibrillated cellulose (MFC/NFC) aqueous suspensions were investigated in oscillation and steady-flow modes and were compared with the morphology of the studied materials. The flow instabilities, which introduce an error in the rheological measurements, were discovered during flow measurements. A wall-slip (interfacial slippage on the edge of geometry tools and suspension) was detected at low shear rates for two types of NFC suspensions while applying cone-plate geometry. A roughening of the tool surfaces was performed to overcome the aforementioned problem. Applying to TEMPO-oxidized NFC, a stronger suspension response was detected at low shear rates with higher values of measured shear stress. However, a shear banding (localization of shear within a sample volume) became more pronounced. The use of serrated tools for enzymatically hydrolyzed NFC produced lower shear stress at the moderate shear rates, which was influenced by water release from the suspension.

1. Introduction

The use of nanocellulose has gained much interest lately, especially in such areas as composites, packaging, adhesives, biomedicine, automotive *etc*. Since it is a renewable and biodegradable material, possessing specific properties, it has a great potential for industrial application.

Nanofibrillated cellulose (NFC), also called microfibrillated cellulose (MFC), is a cellulosic material with lateral dimensions in nanometer scale (≤100 nm), which is usually isolated from cell wall of wood or plants by mechanical fibrillation. Due to a high energy demand during such process an enzymatic (Henriksson, Henriksson, Berglund, & Lindström, 2007; Pääkkö et al., 2007) or chemical (Saito, Nishiyama, Putaux, Vignon, & Isogai, 2006) treatments are commonly used to facilitate nanofibrils separation. NFC is usually extracted as aqueous cellulosic suspensions (1–2 wt.%) and is used further without drying, since the latest promotes irreversible agglomeration of nanofibrils, known as hornification. Therefore, the research has been focusing lately on the properties of cellulose suspensions, especially on their rheological behavior.

A number of studies have been performed on the rheology of NFC suspensions over the last few decades. Research has been conducted on suspensions, produced using: ultrasonication (Chen et al., 2013), mechanical disintegration (Agoda-Tandjawa et al., 2010; Karppinen et al., 2012; Pahimanolis et al., 2011; Saarinen, Lille, & Seppälä, 2009), enzymatic treatment (Charani, Dehghani-Firouzabadi, Afra, & Shakeri, 2013; Pääkkö et al., 2007), TEMPO (2,2,6,6-tetramethylpiperidine-1-oxyl)-mediated oxidation (Lasseuguette, Roux, & Nishiyama, 2008; Saito, Kimura, Nishiyama, & Isogai, 2007), carboxymethylation (Naderi, Lindström, & Sundström, 2014) *etc*. Various sources of cellulosic fibers were used: hardwood (Chen et al., 2013; Karppinen et al., 2012; Pahimanolis et al., 2011; Saarinen et al., 2009; Saito et al., 2007), softwood (Pääkkö et al., 2007), sugar beet (Agoda-Tandjawa et al., 2010; Lowys, Desbrières, & Rinaudo, 2001), kenaf (Charani et al., 2013) *etc*. These studies have mostly focused on the determination of storage and loss moduli (G' and G'', respectively) from the linear viscoelastic regions during oscillation measurements and viscosity (η) and/or shear stress (σ) during the flow measurements.

It was much reported that NFC suspensions exhibit gel-like properties ($G' \gg G''$) even at low concentrations, *e.g.*, 0.125 wt.% (Pääkkö et al., 2007), and have a shear-thinning and thixotropic

* Corresponding author. Tel.: +33 4 56 52 01 95; fax: +33 4 56 52 01 97.
E-mail addresses: oleksandr.nechyporchuk@lgp2.grenoble-inp.fr (O. Nechyporchuk), naceur.belgacem@pagora.grenoble-inp.fr (M.N. Belgacem), frederic.pignon@ujf-grenoble.fr (F. Pignon).

http://dx.doi.org/10.1016/j.carbpol.2014.05.092
0144-8617/

behaviour (Dinand, Chanzy, & Vignon, 1996; Klemm et al., 2011; Pääkkö et al., 2007; Saito et al., 2007). A strong influence of concentration (Charani et al., 2013; Chen et al., 2013; Pääkkö et al., 2007) and an effect of pH (Pääkkö et al., 2007) on the rheological properties of NFC suspensions were also described. NFC is known to have a complex entangled network and the flocculation in flow was studied in several works (Karppinen et al., 2012; Saarinen et al., 2009). Some researchers observed the flow curves containing two shear-thinning regions with a viscosity plateau between them (Agoda-Tandjawa et al., 2010; Iotti, Gregersen, Moe, & Lenes, 2011), which was supposed to occur due to structural changes of the NFC suspension. Karppinen et al. (2012) related such a feature with the changes off locks' structure during the flow, detected using digital camera.

In this work the rheological behavior of the NFC suspensions was studied in oscillation and stepped flow modes. The influence of the used enzymes and their concentrations, oxidation, as well as the other process conditions were analyzed. Saarinen et al. (2009) and Puisto, Illa, Mohtaschemi, & Alava (2012) mentioned the problem of the wall-slip and shear banding in the fibrous suspensions while performing the rheological studies of NFC. Nevertheless, as far as the authors of the present work are aware, no extensive investigation was done to study these phenomena in NFC suspensions. To have more comprehensive understanding of the occurred effects several geometries in combination with visual observations using digital camera were used. To attain the visualization during the experiments, a jet of NFC colored with titanium dioxide (TiO_2) was introduced into the volume of the studied materials.

2. Experimental

2.1. NFC production

The NFC suspensions were produced from bisulfite pulp (Quality 2100, Domsjö Fabriker AB; alpha-cellulose of 93%; DP of 780). Two approaches were used comprising enzymatic and TEMPO-mediated oxidation treatments. For the first one the pulp was extensively refined in the PFI mill for 40,000 revolutions, enzymatically treated (at 50 °C, in 0.05 M acetate buffer, pH 5, during 2 h) and finally grinded using Masuko Supermasscolloider (model MKZA6-2, disk model MKG-C80) at 2500 rpm for 60 passes. Two enzymes were employed separately: Celluclast® 1.5 L (Novozymes A/S, Denmark; 700 endoglucanase units (EGU)/g) using concentrations of 2.1; 10.5 and 21.0 EGU/g of cellulose (enz-C2.1; enz-C10.5 and enz-C21.0 samples, respectively), and FiberCare® R (Novozymes A/S, Denmark; 4700 endocellulase units (ECU)/g) using concentrations of 21; 210 and 315 ECU/g of cellulose (enz-F21; enz-F210 and enz-F315 samples, respectively). The suspensions were heated at 80 °C for 15 min to stop the enzymatic activity, cooled down to 25 °C and the pH was adjusted to 7 using 3 M NaOH. The samples were prepared with the concentration of 2.00 wt.%. Chloroform at 0.01 wt.% was used as a biocide.

One sample (enz-F21-H) was refined in PFI mill, treated with FiberCare® R applying 21 ECU/g of cellulose, grinded for 1 h through Masuko Supermasscolloider (6 L of suspension), equipped with recirculation pump, and then passed two times through homogenizer GEA Panther NS3006L (1000 and 1500 bar, respectively). Due to some water, remaining in the homogenizer before the processing, the NFC suspension was diluted slightly. The resulted concentration was measured and found to be 1.75 wt.%.

For TEMPO-mediated oxidation TEMPO/NaBr/NaClO system (0.1; 1 and 5 mmol/g of cellulose, respectively; pH of 10; at 25 °C) was used (ox-TEMPO sample). The oxidized cellulose was filtered on a Büchner funnel using a nylon sieve with a mesh size of 1 μm and washed with deionized water until the filtrate conductivity value was below 5 μS/cm. Finally, cellulose was redispersed in deionized water at 1.00 wt.% (at higher concentrations the processing of the samples become complicated due to high viscosity) and ground with Masuko Supermasscolloider for 60 passes.

To study the effect of concentration, the NFC suspensions were concentrated using centrifuge Sigma 6-16KS at 10,000 rpm for 15 min. The dry content was measured gravimetrically, and then NFC was redispersed in deionized water for a desired concentration.

All the samples were stored in a fridge at 4 °C and left overnight at room temperature (~23 °C) before the measurements.

2.2. Microscopy observations

The morphology of the NFC suspensions was studied using optical and atomic force microscopy. For the optical microscopy the cellulose suspensions were diluted with deionized water till 0.2 wt.%. A drop of suspension was placed on glass and covered with a coverslip. Carl Zeiss Axio Imager M1m optical microscope in the transmission mode was used to observe the samples. The images were captured by AxioCam MRc 5 digital camera. For the atomic force microscopy the NFC suspensions were diluted till 10^{-3} wt.%. A drop of the suspension was spilt on the mica disc and dried at room temperature. The images were captured in the tapping mode using Dimension Icon® Atomic Force Microscope under ambient temperature and relative humidity with an OTESPA cantilever. At least four different areas at the sample were scanned. Nanoscope III and ImageJ image processing software were used for an evaluation of the obtained images.

2.3. Rheological measurements

The measurements were carried out using a stress-controlled rheometer DHR-3 (TA Instruments). Initially, the recessed concentric cylinders (cup diameter of 30 mm; bob diameter of 28 mm; operating gap of 4 mm) were used to study the NFC suspensions in the oscillation and flow modes. The oscillation strain sweeps from 0.01 to 10% at the angular frequency of 1 rad/s were carried out to define the linear viscoelastic regimes. Then the oscillation frequency sweeps in the range of 0.1–100 rad/s at 0.1 strain% for ox-TEMPO and at 0.05 strain% for all the other samples were performed. The steady flow was measured applying the shear rate from 0.001 to 1000 s^{-1} with a step of one decade. The values of η and σ were picked out after achieving the steady state.

To study the shear instabilities during the rheological measurements, a visualization device of the strain field inside the sample was used, as reported elsewhere (Pignon, Magnin, & Piau, 1996). Smooth cone and plate geometries (roughness of ~0.8 μm) or serrated by attaching sandpaper (roughness of ~120 μm) were used. The cone (truncation gap of 130 μm (without sandpaper) and 570 μm (with sandpaper); angle of 4°21′ 30″; diameter of 49 mm) was pierced at a distance of 3 mm from the edge and a vertical filament of the suspension, colored with titanium dioxide powder, was introduced into the volume of the sample (see Fig. 1).

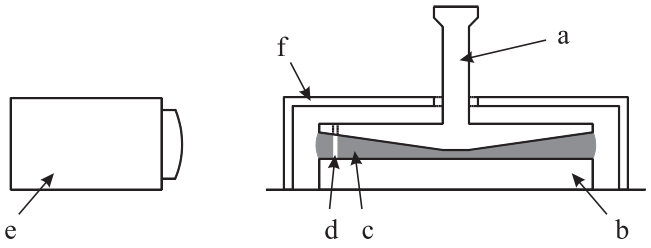

Fig. 1. Schematic diagram of the setup for the rheological measurements combined with visualization of the strain field inside the sample: truncated cone (a); plate (b); studied NFC suspension (c); filament of the NFC suspension, colored with titanium dioxide (d); CCD camera (e); transparent cover to prevent water evaporation (f).

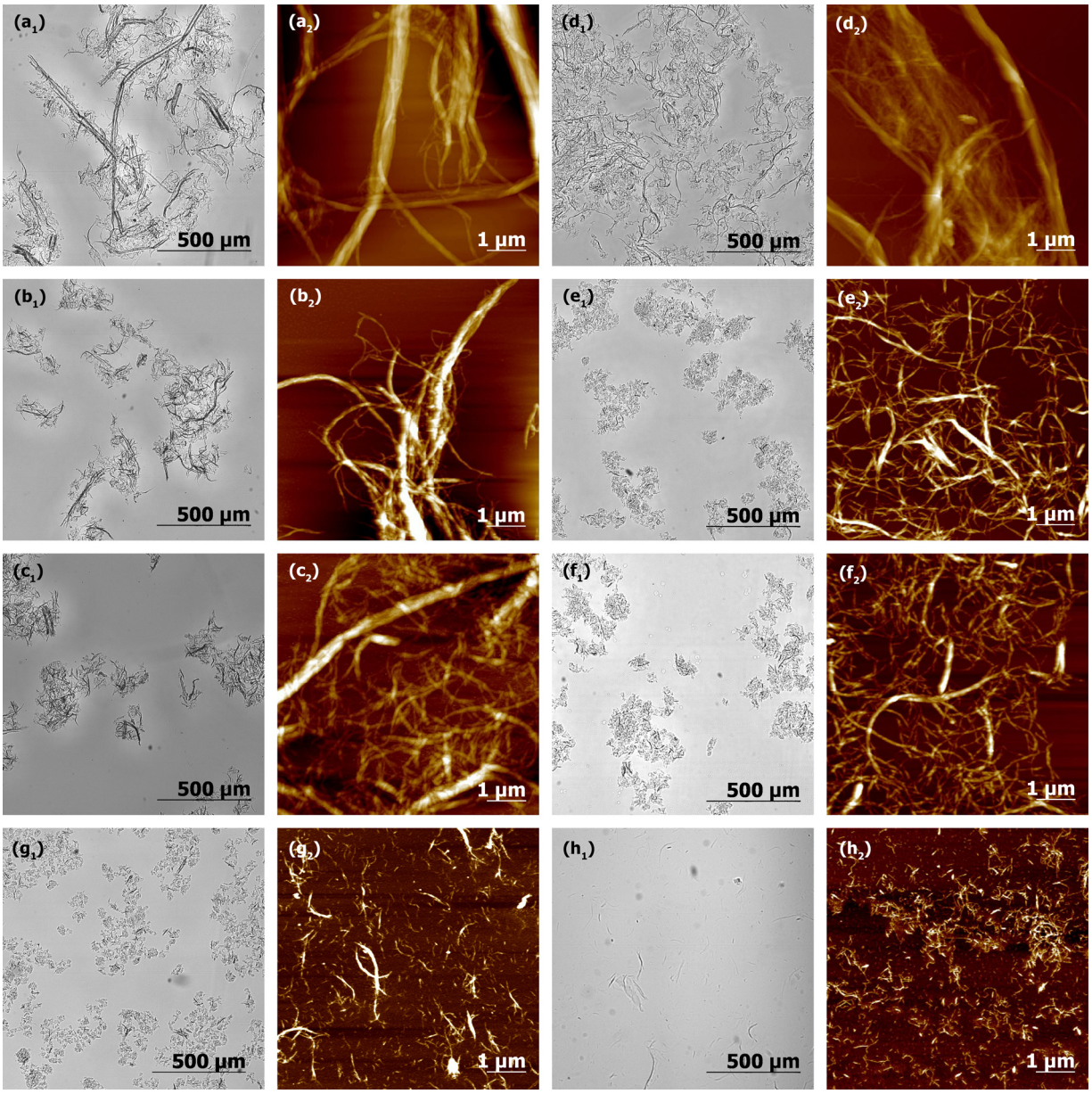

Fig. 2. Optical microscopy (subscript 1) and atomic force microscopy (subscript 2) images of: enz-C2.1 (a); enz-C10.5 (b); enz-C21 (c); enz-F21 (d); enz-F210 (e); enz-F315 (f); enz-F21-H (g); and ox-TEMPO (h) samples.

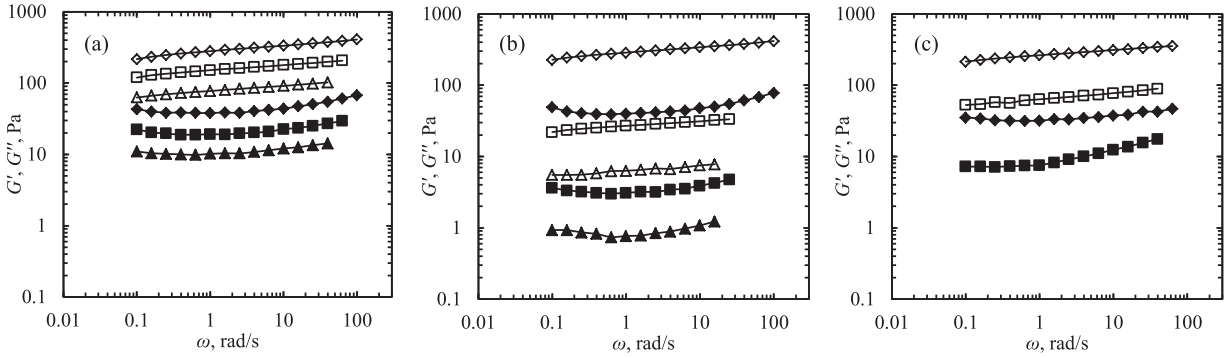

Fig. 3. Storage (empty symbols) and loss moduli (filled symbols) as a function of oscillation frequency of: (a) enz-F21 (◊,♦), enz-F210 (□,■), enz-F315 (△, ▲); (b) enz-C2.1 (◊, ♦), enz-C10.5 (□,■), enz-C21 (△,▲) (all the samples at 2.00 wt.% concentration); (c) enz-F21-H (◊,♦) of 1.75 wt.% and ox-TEMPO (□,■) of 1.00 wt.%. Performed using concentric cylinders geometry.

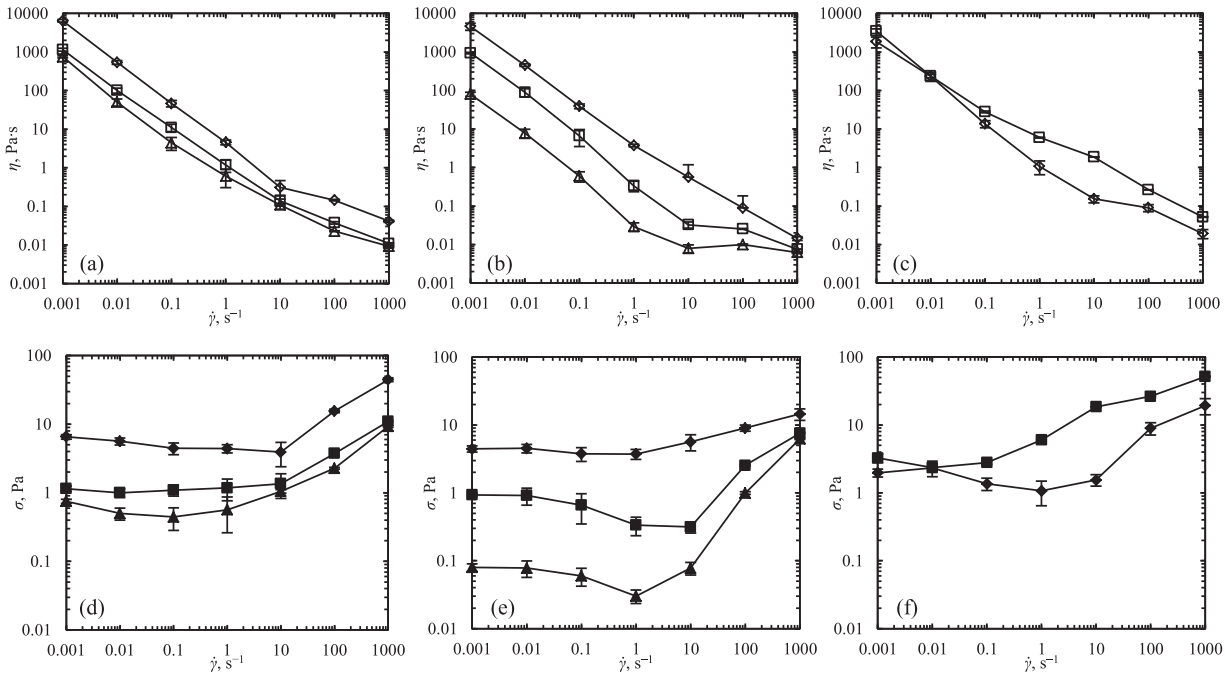

Fig. 4. Viscosity (a–c) and shear stress (d–f) as a function of shear rate for: (a and d) enz-F21 (◊,♦), enz-F210 (□,■), enz-F315 (△,▲); (b and e) enz-C2.1 (◊,♦), enz-C10.5 (□,■), enz-C21 (△,▲); (c and f) enz-F21-H (◊,♦), ox-TEMPO (□,■). Performed using concentric cylinders geometry.

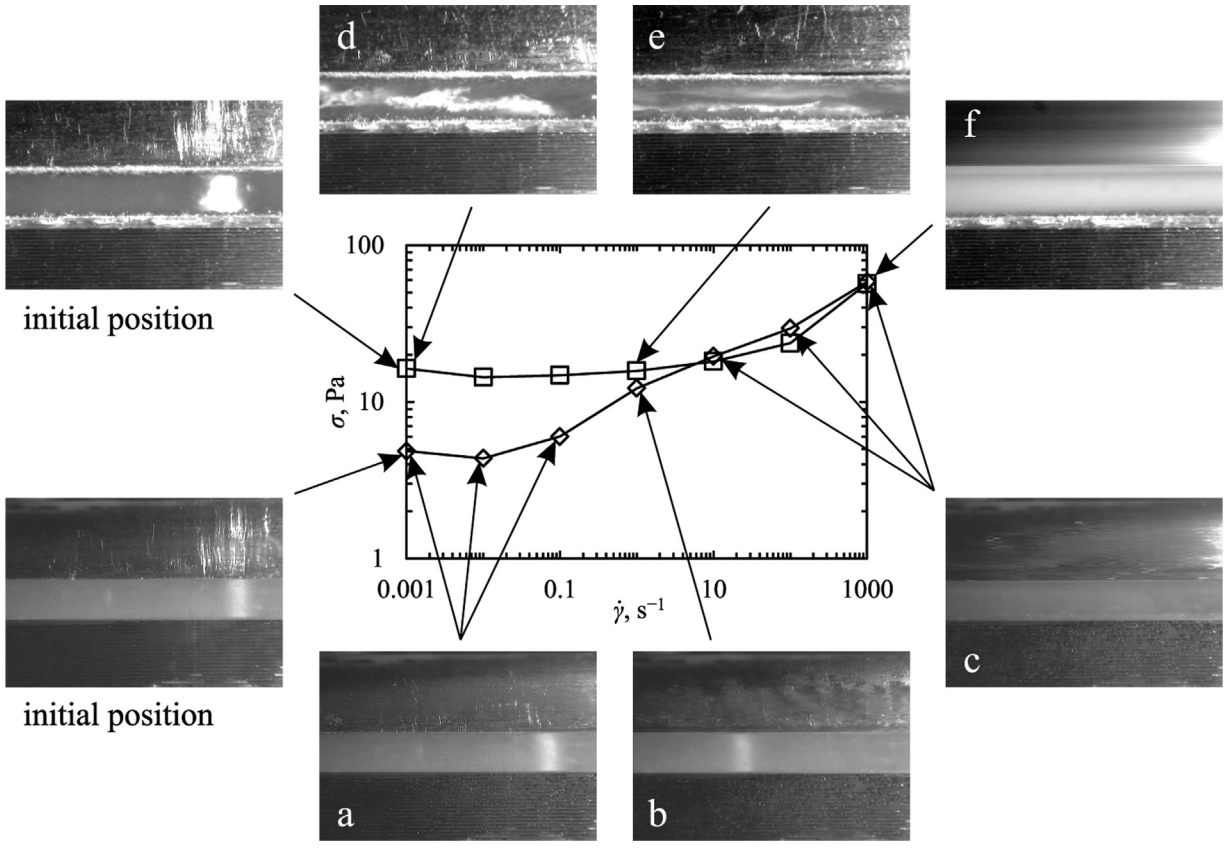

Fig. 5. Shear stress as a function of shear rate together with visualization of the flow behavior of ox-TEMPO NFC sample using serrated (□) and non-serrated (smooth) (◊) cone-plate geometries. Illustration of the occurred phenomena applying non-serrated geometries: wall-slip on the boundary of the NFC suspension and the cone (a); wall-slip on the boundaries of the NFC suspension and both cone and plate (b); sample flow, shear banding detected (not noticeable from the photograph) (c). Occurred phenomena applying serrated geometries: sample flow (d); shear banding with a fracture between the moving and stagnant NFC suspension parts (e); sample flow (f).

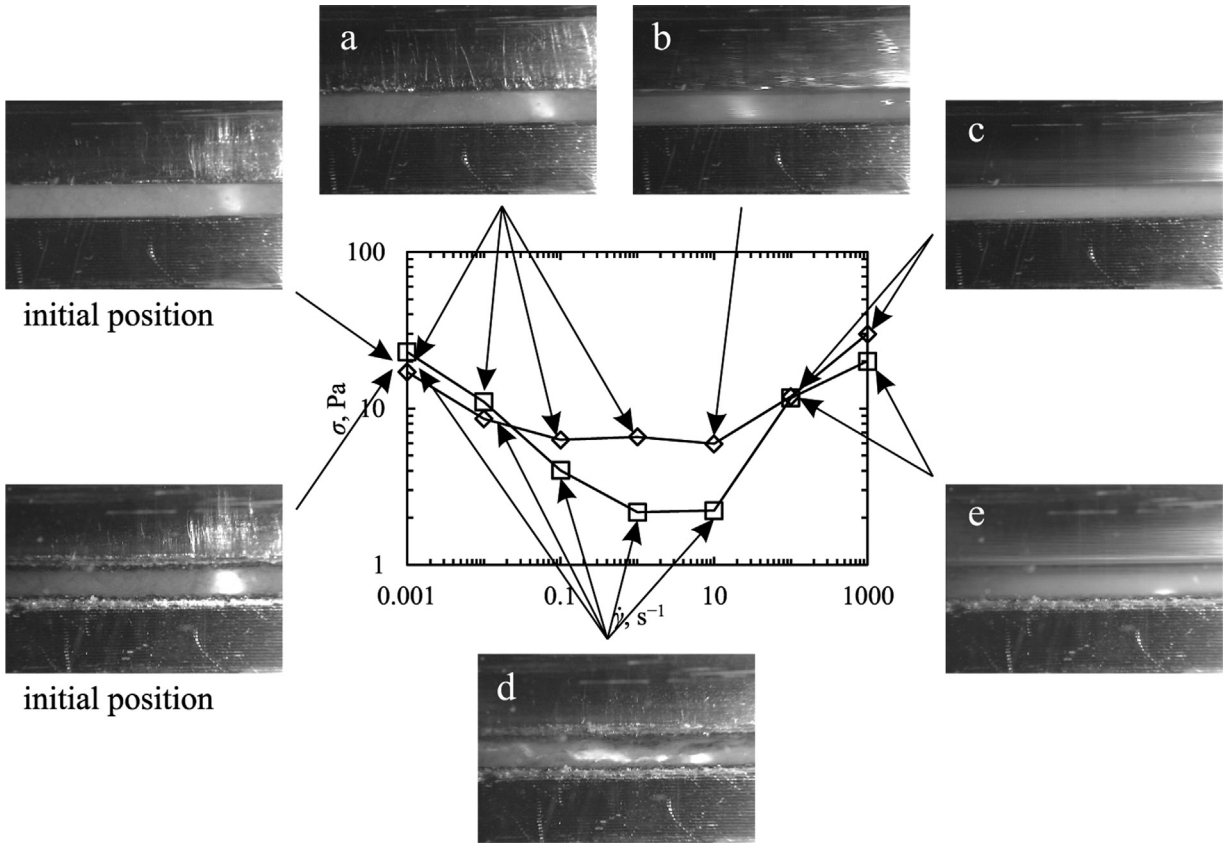

Fig. 6. Shear stress as a function of shear rate together with visualization of the flow behavior of enz-F21-H NFC sample using serrated (□) and non-serrated (smooth) (◊) cone-plate geometries. Illustration of the occurred phenomena applying non-serrated geometries: wall-slip on the boundary of the NFC suspension and the cone (a); wall-slip on the boundaries of the NFC suspension and both cone and plate (b); sample flow (c). Occurred phenomena applying serrated geometries: wall-slip at the boundary of the NFC suspension and the cone, the lubrication layer was noticeable due to water release from the sample (d); sample flow (e).

A transparent cover was used to prevent the water evaporation. Displacement of the colored vertical filament was monitored outside using CCD camera.

Finally, ox-TEMPO and enz-F21-H samples of different cellulose concentrations were examined in oscillation mode using serrated cone-plate geometry. All the measurements were carried out at controlled temperature of 23 °C.

3. Results and discussion

3.1. Morphological properties

In order to have an idea about the morphology of the studied materials before the rheological characterization they were analyzed using microscopy techniques. Fig. 2 shows the optical and atomic force microscopy images of the studied MFC/NFCs. All enzymatically treated samples (Fig. 2a–g) possess flocculated heterogeneous structure, as seen from the optical microscopy images. The flock size decreases with an increase of the enzymatic concentration and a fine network of nanofibrils is observed. During the enzymatic hydrolysis a decrease of the degree of polymerization was observed (not shown in this work), which was stronger when applying Celluclast® 1.5 L. The use of FiberCare® R allowed the enzymes concentration to be increased, inhibiting more the fibers depolymerization (saccharification). Thus, obtained enz-F210 and enz-F315 samples had the nanofibrils with lateral dimensions starting from 40 nm (Fig. 2e and f).

As a result of TEMPO-mediated oxidation, the nanofibrils of 10 nm in diameter were produced. However, some residual fibers were still present, observed using optical microscopy (Fig. 2h_1).

3.2. Rheological properties

3.2.1. Oscillation measurements

During the oscillation strain sweeps (not shown in figures) the critical strain was much higher for ox-TEMPO (~1 strain%) comparing to enzymatically treated samples (~0.1 strain%), for which it was almost independent of the enzymes types and their concentrations. The storage and loss moduli as a function of oscillation frequency are shown in Fig. 3. The G' and G'' were plotted while the raw phase was below 90° indicating no influence of the inertial effects.

It is evident that all the suspensions exhibit gel-like properties ($G' \gg G''$) in a large range of frequencies. Surprisingly, with the increase of enzymatic concentration the dynamic moduli decrease despite the higher fibrillation and, hence, the higher specific surface area of fibrous elements. However, it can be explained by the enzymatic depolymerization of cellulose.

The NFC suspensions treated with FiberCare® R (Fig. 3a), despite the higher enzymatic concentration applied, resulted in stronger networks comparing to that of Celluclast® 1.5 L (Fig. 3b). Comparing the two types of the applied enzymes, it should be noticed that Celluclast® 1.5 L is an enzyme mixture composed of Trichoderma reesei fungus containing endoglucanases, exo-glucanases, cellobiohydrolases, and β-glucosidases, while FiberCare® R is a monocomponent endoglucanase. Thereby, the former degrades cellulose to elementary sugars in a stronger manner due to its composition. Consequently, the use of Celluclast® 1.5 L decreases more the viscoelasticity of the NFC suspensions.

The dynamic moduli of enz-F21-H are practically equal to enz-F21, however the concentrations of the samples are 1.75 *vs.*

2.00 wt.%, respectively, indicating the stronger fibrous network of the first. The storage and loss moduli of ox-TEMPO (1.00 wt.%) are similar to that of enz-F315 (2.00 wt.%). The NFC concentration effect is presented in Section 3.2.4.

3.2.2. Flow properties

All the studied NFC suspensions exhibit a shear-thinning behavior, as seen from the flow curves in Fig. 4. A decrease of viscosity is observed as the shear rate ($\dot{\gamma}$) increases and for some samples a Newtonian plateau can be noticed at shear rates of 10–100 s^{-1}. The similar behavior was reported in the other studies (Agoda-Tandjawa et al., 2010; Iotti et al., 2011; Pääkkö et al., 2007). The shear stress decreases slightly till the intermediate shear rates (0.1–10 s^{-1}) and is followed by a strong increase for the range of 10–1000 s^{-1}. Similar behavior was previously reported by Karppinen et al. (2012).

The difference between the flow behavior of the studied samples is similar with that of the storage and loss moduli described in Section 3.2.1.

3.2.3. Visualization of shear instabilities

To study the strain field inside the bulk of the NFC suspensions the truncated cone and plate geometry in combination with visual observations using CCD camera were applied. The introduced vertical filament of the suspension, colored with TiO_2 (as shown in Fig. 1), promoted the representation of the taking place effects.

It is apparent from Fig. 5 (see photographs below the graph) that when using non-serrated (smooth) cone-plate geometry at low shear rates (0.001–0.1 s^{-1}) the ox-TEMPO sample remained almost not deformed, since the wall-slip occurred (video of the flow behavior of newly introduced NFC suspensions at each characteristic shear rate is shown in Supplementary data). Initially, a small deformation happened at the beginning of the experiment which is seen from a slight deviation from the vertical position of the colored rod. The further shear forces did not induce the deformation, producing the wall-slip on the boundary of the NFC and the cone.

At the shear rate of 1 s^{-1} the slippage on the edge between the suspension and both cone and plate occurred (Fig. 5b). Moreover, no deformation of the bulk took place so that the NFC rotated preserving the colored rod shape. Only achieving the shear rate of 10 s^{-1} the bulk deformation was attained (see Fig. 5c). Nevertheless, the suspension did not flow uniformly: the fast and slow flowing regions were observed, which is known as shear banding phenomenon. At higher shear rates, above 10 s^{-1}, the suspension flows within all the gap of the tools geometry, which is more relevant as a volume property of the sample.

The shape of the shear stress *vs.* shear rate dependence of ox-TEMPO sample measured using smooth cone-plate geometry (Fig. 5) is similar to that of measured using concentric cylinders (Fig. 4f). Thereby, it is assumed that in the latter the wall-slip and shear banding phenomena could also took place.

The wall-slip is known to occur in the fibrous suspensions. It originates from the displacement of a disperse phase from solid boundaries, which creates a lubrication effect (Barnes, 1995). As a result, a very narrow layer of the suspension (typically 0.1–10 μm) at the boundary is subjected to flow; thereby, it is considered sometimes as shear banding. Since this layer of the suspension is very thin, it is almost imperceptible and appears as a wall-slip.

Saarinen et al. (2009) showed the influence of the geometry gap on the viscoelastic properties of the NFC suspensions. They associated the results divergence with the wall-slip. To hinder the wall-slip phenomena while studying different kinds of materials the roughening of the geometry surfaces has been sufficiently applied, *e.g.*, by sandblasting (Buscall, McGowan, & Morton-Jones, 1993) or attaching sandpaper (Pignon et al., 1996). Iotti et al. (2011) used plate-plate geometry with roughened base plate in order to prevent the wall-slip while studying the NFC suspensions. However, no results in their work were reported showing whether it was efficient or not to hinder the slip.

In this work sandpaper was used to form the rough surfaces on the cone and plate as described in Section 2.3. The use of serrated geometries prevented the slip while testing the ox-TEMPO, as shown in Fig. 5 (the photographs above the graph). The resulted values of the shear stress at low shear rates are notably higher comparing to that of non-serrated geometry and can be considered

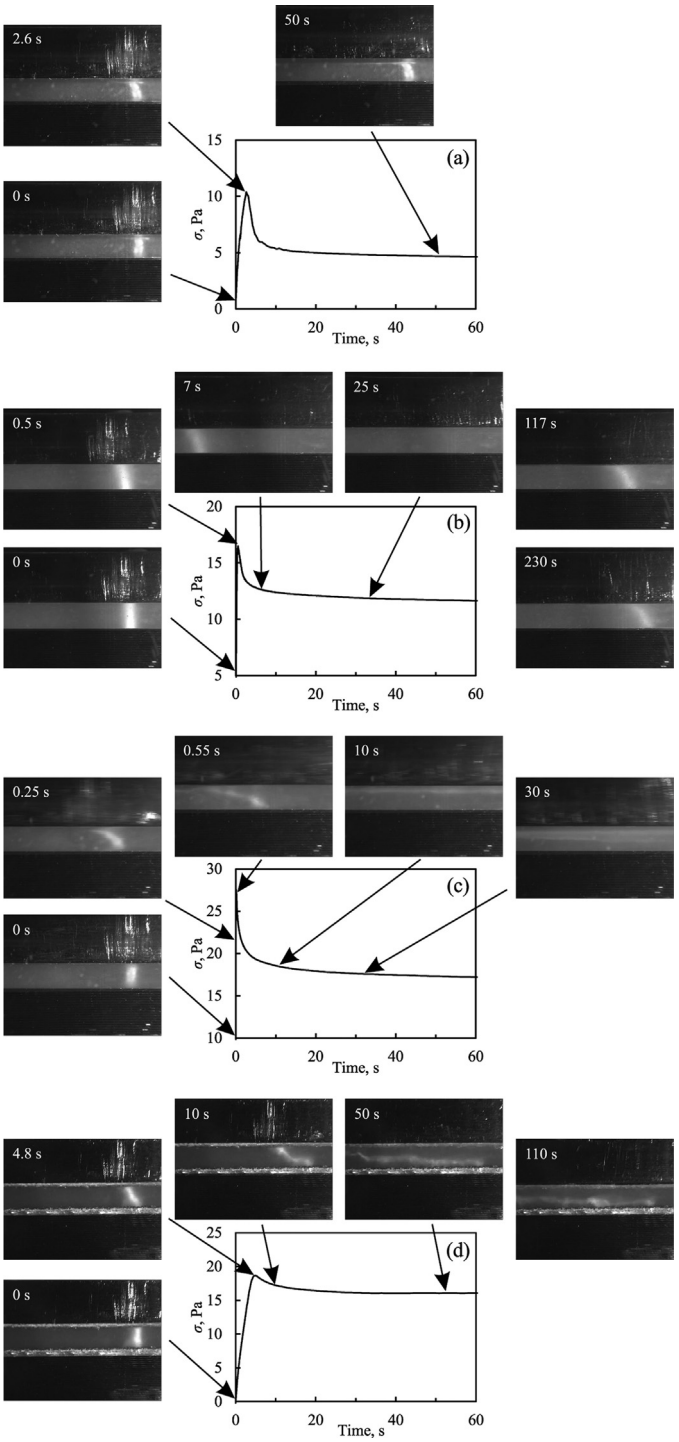

Fig. 7. Shear stress as a function of time of ox-TEMPO NFC sample measured at shear rate of: 0.1 s^{-1} (a and d); 1 s^{-1} (b) and 10 s^{-1} (c) using non-serrated (a–c) and serrated (d) cone-plate geometries. The time when picture was taken is indicated in the top left part of the photograph.

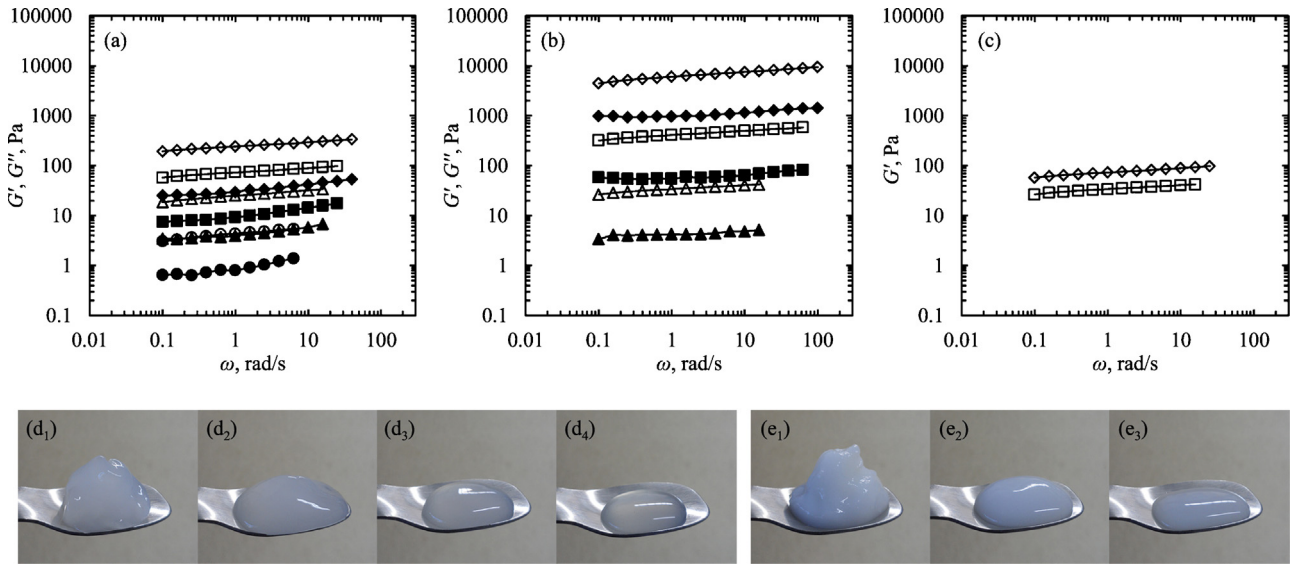

Fig. 8. Viscoelastic properties and digital camera photographs of the NFC suspensions at different concentrations. Storage (empty symbols) and loss moduli (filled symbols) as a function of oscillation frequency of: ox-TEMPO NFC sample (a) at 1.25 wt.% (◊,♦); 1.00 wt.% (□,■); 0.75 wt.% (△,▲); 0.50 wt.% (○,●); enz-F21-H NFC sample (b) at 3 wt.% (◊,♦), 2 wt.% (□,■) and 1 wt.% (△,▲); and ox-TEMPO (◊) and enz-F21-H (□) NFC samples (c) both at 1.00 wt.%. Photographs of: ox-TEMPO at 1.25 wt.% (d_1), 1.00 wt.% (d_2), 0.75 wt.% (d_3), 0.50 wt.% (d_4) and enz-F21-H at 3 wt.% (e_1), 2 wt.% (e_2) and 1 wt.% (e_3).

as more correct since the sample is subjected to the deformation. However, the fracture of the bulk was observed, especially it was evident at the shear rate of 1 s^{-1} (Fig. 5e). It resulted in the localization of the flow within a fine layer in the middle of the bulk.

Fig. 6 (the photographs above the graph) shows that the wall-slip occurred for enz-F21-H sample as well when applying the smooth geometry. It was observed even at the shear rate of 1 s^{-1} at which the suspension remained not deformed (Fig. 6a). At 10 s^{-1} the slippage at two boundaries, similarly to that described above for ox-TEMPO at 1 s^{-1}, took place without causing the deformation of the bulk (Fig. 6b). The flow of the sample was detected at 100 s^{-1} when the shear rate started to increase as a function of shear rate (Fig. 6c).

The use of serrated cone and plate (see Fig. 6, photographs below the graph) increased slightly the values of the shear stress at low shear rates. However, then a drastic decrease was observed since the sand granules were likely to alter the structure of the NFC, releasing water from the NFC suspension and creating the lubrication layer, localized between the NFC and the cone (Fig. 6d). As a result, the flow was localized in the top layer of the suspension. At this range of shear rates (0.001–10 s^{-1}) the shear stress level corresponds to the stress in a thin top layer of the bulk and is not representative of a volume property of the sample. By the further increase of shear rate (above 100 s^{-1}) the flow of the all volume of the enz-F21-H sample was achieved (Fig. 6e) and the shear stress reached the same values, which were obtained with non-serrated tools.

Fig. 7 shows the ox-TEMPO suspension analyzed at different characteristic shear rates. For each test a new portion of the sample was placed and the shear stress was analyzed as a function of step time. The sample deformation can be monitored in video available in Supplementary data. Subjecting the sample to the shear, the colored rod passed from the vertical to slightly inclined position till the yield stress, corresponding to the maximum of the stress–time curve (*e.g.*, in Fig. 7a at time of 2.6 s). After this, at different shear rates: a wall slip at upper boundary (Fig. 7a); a wall slip at both upper and lower boundaries (Fig. 7b) and the flow within all the sample volume (Fig. 7c) occurred. Fig. 7d represents the use of serrated geometry and the changes of ox-TEMPO structure at different time points. After reaching the yield stress a fracture of the sample bulk occurred. The time of the image capturing from the beginning of the test is indicated in the top left position on the photograph.

3.2.4. *Effect of the NFC concentration*

Viscoelastic properties of ox-TEMPO (Fig. 8a) and enz-F21-H (Fig. 8b) were investigated at different cellulose concentrations. The storage and loss moduli increased dramatically with the increase of cellulose concentration. By changing the mass fraction of ox-TEMPO from 0.75 to 1.25 wt.% the storage modulus increased for one order of magnitude. In the case of enz-F21-H at the oscillation frequency of 1 rad/s G' changed from 34 to 6023 Pa by varying the concentration from 1 to 3 wt.%. The drastic change of the dynamic moduli with a slight variation of cellulose concentration is in agreement with the other studies (Agoda-Tandjawa et al., 2010; Charani et al., 2013; Dimic-Misic et al., 2013; Iotti et al., 2011; Lowys et al., 2001; Pääkkö et al., 2007).

Fig. 8c shows G' of ox-TEMPO and enz-F21-H both at 1 wt.% for comparison. It is seen, that the former has a stronger fibrous network which can be explained by nanofibrils lower dimensions, shown in Section 3.1. The smaller are the particles of a colloidal suspension, the higher is the volume fraction, which is the relevant parameter.

4. Conclusions

An extensive rheological study of the NFC aqueous suspensions in oscillation and steady-state flow modes was performed. All the suspensions exhibited gel-like, shear-thinning properties. It was shown that the concentration and the type of applied enzymes have an influence on the rheological behavior of the tested suspensions. The dynamic moduli as well as viscosity and shear stress decreased with the increase of enzymatic charge which is likely to occur due to cellulose saccharification together with nanofibrils separation. The NFC obtained from TEMPO-mediated oxidation resulted in stronger fibrous network, which was confirmed by smaller nanofibril dimensions observed using microscopy techniques.

As far as the authors of this work are aware, it is the first published study devoted to the investigation of the wall-slip and shear

banding phenomena in NFC suspensions. When using the smooth geometries, the flow instabilities were detected by flow observation. A wall-slip took place at wide range of shear rates for two types of NFC suspensions: produced using enzymatic and TEMPO-mediated oxidation pretreatments. Therefore, the obtained values are considered to comprise an error, introduced by the wall-slip. To prevent this slip the roughening of the geometry tools was performed. It resulted in more accurate measurements; however, only for TEMPO-oxidized NFC suspension. The use of serrated tools did not prevent the wall-slip of enzymatically pretreated NFC.

This study shows that for two types of NFC suspensions, produced using enzymatic and TEMPO-mediated oxidation pretreatments, examined in this work, there is a distortion of the measured flow properties, induced by flow instabilities, especially at low shear rates (0.001–1 s^{-1}). Certainly, the use of other raw materials or processing conditions for the production of NFC, other rheometer geometries as well as the operating gap can make an influence on the resulted data. Therefore, diverse systems to prevent such phenomena should be investigated. The use of grooved cup and vane geometry appears of great interest in this context.

Acknowledgments

This work has been performed in scope of International Doctoral Program in Functional Materials (IDS-FunMat, Erasmus Mundus) funded by Université Joseph Fourier, Grenoble, France. Sincere gratitude is expressed to Novozymes A/S and Domsjö Fabriker AB for providing the samples of their products. Laboratoire Rhéologie et Procédés (LRP) is a part of the LabEx Tec 21 (Investissements d'Avenir–grant agreement no. ANR-11-LABX-0030). Laboratoire Génie des Procédés Papetiers (LGP2) is a part of the LabEx Tec 21 (Investissements d'Avenir–grant agreement no. ANR-11-LABX-0030) and of the Energies du Futur and PolyNat Carnot Institutes.

Appendix A. Supplementary data

Supplementary material related to this article can be found, in the online version, at http://dx.doi.org/10.1016/j.carbpol.2014.05.092.

References

Agoda-Tandjawa, G., Durand, S., Berot, S., Blassel, C., Gaillard, C., Garnier, C., & Doublier, J.-L. (2010). Rheological characterization of microfibrillated cellulose suspensions after freezing. *Carbohydrate Polymers*, *80*(3), 677–686. http://dx.doi.org/10.1016/j.carbpol.2009.11.045

Barnes, H. A. (1995). A review of the slip (wall depletion) of polymer solutions, emulsions and particle suspensions in viscometers: Its cause, character, and cure. *Journal of Non-Newtonian Fluid Mechanics*, *56*(3), 221–251. http://dx.doi.org/10.1016/0377-0257(94)01282-M

Buscall, R., McGowan, J. I., & Morton-Jones, A. J. (1993). The rheology of concentrated dispersions of weakly attracting colloidal particles with and without wall slip. *Journal of Rheology*, *37*(4), 621–641. http://dx.doi.org/10.1122/1.550387 (1978-Present)

Charani, P. R., Dehghani-Firouzabadi, M., Afra, E., & Shakeri, A. (2013). Rheological characterization of high concentrated MFC gel from kenaf unbleached pulp. *Cellulose*, *20*(2), 727–740. http://dx.doi.org/10.1007/s10570-013-9862-1

Chen, P., Yu, H., Liu, Y., Chen, W., Wang, X., & Ouyang, M. (2013). Concentration effects on the isolation and dynamic rheological behavior of cellulose nanofibers via ultrasonic processing. *Cellulose*, *20*(1), 149–157. http://dx.doi.org/10.1007/s10570-012-9829-7

Dimic-Misic, K., Puisto, A., Gane, P., Nieminen, K., Alava, M., Paltakari, J., & Maloney, T. (2013). The role of MFC/NFC swelling in the rheological behavior and dewatering of high consistency furnishes. *Cellulose*, *20*(6), 2847–2861. http://dx.doi.org/10.1007/s10570-013-0076-3

Dinand, E., Chanzy, H., & Vignon, M. R. (1996). Parenchymal cell cellulose from sugar beet pulp: Preparation and properties. *Cellulose*, *3*(1), 183–188. http://dx.doi.org/10.1007/BF02228800

Henriksson, M., Henriksson, G., Berglund, L. A., & Lindström, T. (2007). An environmentally friendly method for enzyme-assisted preparation of microfibrillated cellulose (MFC) nanofibers. *European Polymer Journal*, *43*(8), 3434–3441. http://dx.doi.org/10.1016/j.eurpolymj.2007.05.038

Iotti, M., Gregersen, Ø. W., Moe, S., & Lenes, M. (2011). Rheological studies of microfibrillar cellulose water dispersions. *Journal of Polymers and the Environment*, *19*(1), 137–145. http://dx.doi.org/10.1007/s10924-010-0248-2

Karppinen, A., Saarinen, T., Salmela, J., Laukkanen, A., Nuopponen, M., & Seppälä, J. (2012). Flocculation of microfibrillated cellulose in shear flow. *Cellulose*, *19*(6), 1807–1819. http://dx.doi.org/10.1007/s10570-012-9766-5

Klemm, D., Kramer, F., Moritz, S., Lindström, T., Ankerfors, M., Gray, D., & Dorris, A. (2011). Nanocelluloses: A new family of nature-based materials. *Angewandte Chemie International Edition*, *50*(24), 5438–5466. http://dx.doi.org/10.1002/anie.201001273

Lasseuguette, E., Roux, D., & Nishiyama, Y. (2008). Rheological properties of microfibrillar suspension of TEMPO-oxidized pulp. *Cellulose*, *15*(3), 425–433. http://dx.doi.org/10.1007/s10570-007-9184-2

Lowys, M.-P., Desbrières, J., & Rinaudo, M. (2001). Rheological characterization of cellulosic microfibril suspensions. Role of polymeric additives. *Food Hydrocolloids*, *15*(1), 25–32. http://dx.doi.org/10.1016/S0268-005X(00)00046-1

Naderi, A., Lindström, T., & Sundström, J. (2014). Carboxymethylated nanofibrillated cellulose: Rheological studies. *Cellulose*, 1–11. http://dx.doi.org/10.1007/s10570-014-0192-8

Pääkkö, M., Ankerfors, M., Kosonen, H., Nykänen, A., Ahola, S., Österberg, M., Lindström, T., et al. (2007). Enzymatic hydrolysis combined with mechanical shearing and high-pressure homogenization for nanoscale cellulose fibrils and strong gels. *Biomacromolecules*, *8*(6), 1934–1941. http://dx.doi.org/10.1021/bm061215p

Pahimanolis, N., Hippi, U., Johansson, L.-S., Saarinen, T., Houbenov, N., Ruokolainen, J., & Seppälä, J. (2011). Surface functionalization of nanofibrillated cellulose using click-chemistry approach in aqueous media. *Cellulose*, *18*(5), 1201–1212. http://dx.doi.org/10.1007/s10570-011-9573-4

Pignon, F., Magnin, A., & Piau, J.-M. (1996). Thixotropic colloidal suspensions and flow curves with minimum: Identification of flow regimes and rheometric consequences. *Journal of Rheology*, *40*(4), 573–587. http://dx.doi.org/10.1122/1.550759

Puisto, A., Illa, X., Mohtaschemi, M., & Alava, M. (2012). Modeling the rheology of nanocellulose suspensions. *Nordic Pulp and Paper Research Journal*, *27*(2), 277–281.

Saarinen, T., Lille, M., & Seppälä, J. (2009). Technical aspects on rheological characterization of microfibrillar cellulose water suspensions. *Annual Transactions of the Nordic Rheology Society*, *17*, 121–130.

Saito, T., Kimura, S., Nishiyama, Y., & Isogai, A. (2007). Cellulose nanofibers prepared by TEMPO-mediated oxidation of native cellulose. *Biomacromolecules*, *8*(8), 2485–2491. http://dx.doi.org/10.1021/bm0703970

Saito, T., Nishiyama, Y., Putaux, J.-L., Vignon, M., & Isogai, A. (2006). Homogeneous suspensions of individualized microfibrils from TEMPO-catalyzed oxidation of native cellulose. *Biomacromolecules*, *7*(6), 1687–1691. http://dx.doi.org/10.1021/bm060154s